International Journal of Disaster Risk Science (2023) 14:751–767
https://doi.org/10.1007/s13753-023-00514-w

www.ijdrs.com
www.springer.com/13753

ARTICLE

# Assessing Global Landslide Casualty Risk Under Moderate Climate Change Based on Multiple GCM Projections

**Xia Wang[1,2] · Ying Wang[1,2] · Qigen Lin[3] · Xudong Yang[4]**

Accepted: 30 September 2023 / Published online: 7 November 2023


## Abstract

Extreme precipitation-induced landslide events are projected to increase under climate change, which poses a serious threat to human lives and property. In this study, a global-scale landslide risk assessment model was established using global landslide data, by considering landslide hazard, exposure, and vulnerability. The global climate model data were then employed to drive the established global landslide risk model to explore the spatial and temporal variations in future landslide risk across the globe as a result of extreme precipitation changes. The results show that compared to the 30-year period from 1971 to 2000, the average annual frequency of landslides triggered by extreme precipitation is projected to increase by 7% and 10%, respectively, in the future 30-year periods of 2031–2060 and 2066–2095. The global average annual casualty risk of landslides is projected to increase from about 3240 to 7670 and 8380, respectively (with growth rates of 140% and 160%), during the 2031–2060 and 2066–2095 periods under the SSP2-4.5 scenario. The top 10 countries with the highest casualty risk of landslides are China, Afghanistan, India, the Philippines, Indonesia, Rwanda, Turkey, Nepal, Guatemala, and Brazil, 60% of which are located in Asia. The frequency and intensity of extreme precipitation will increase under climate change, which will lead to an increase in casualties from landslides in mountainous areas globally, and this risk should be taken seriously. The present study was an attempt to investigate and quantify the impact of global landslide casualty risk under climate change, which still has uncertainty in terms of outcomes, and there remains a need for further understanding in the future of the propagation of uncertainty between the factors that affect the risk.

**Keywords** Casualty risk · Climate change · Extreme precipitation · Global landslides · Multi-GCMs

## 1 Introduction

Landslides are widely distributed around the world and have serious impacts on human society every year (Petley et al. 2007; Budimir et al. 2015). According to the statistics of the Emergency Events Database (EM-DAT), the 631 landslide disaster events recorded from 1980 to 2017 caused 44,541 casualties (CRED 2019). According to the statistics of the global catastrophic landslide database, which spans the years 2004 to 2010 and was established by Petley (2012), an average of 374 catastrophic landslides occurred every year worldwide in that period, causing approximately 4617 casualties annually. Extreme precipitation is an important triggering factor of landslides. The Intergovernmental Panel on Climate Change (IPCC) Sixth Assessment Report (AR6) noted that the warming of the global climate system is clear (IPCC 2021), and the thermodynamic effects of climate change may cause the frequency and intensity of extreme precipitation events to increase (Kharin et al. 2013; Westra et al. 2014), which may affect the occurrence of landslides in some regions of the world with high reliability (Gariano and Guzzetti 2016, 2022). Therefore, projections of global landslide casualty risks of precipitation extremes under climate

✉ Ying Wang
wy@bnu.edu.cn

1 Key Laboratory of Environmental Change and Natural Disaster, Ministry of Education, Beijing Normal University, Beijing 100875, China

2 Academy of Disaster Reduction and Emergency Management, Ministry of Emergency Management and Ministry of Education, Beijing 100875, China

3 Institute for Disaster Risk Management / School of Geographical Sciences, Nanjing University of Information Science & Technology, Nanjing 210044, China

4 China Institute of Geo-Environmental Monitoring, Beijing 100081, China

change scenarios are essential for formulating scientific landslide mitigation strategies.

Risk assessments mainly include three elements: hazard, exposure, and vulnerability (IPCC 2011). Research on landslides is the basic premise for projections of populations at risk of landslides. Some scholars have studied the impacts of climate change on landslides in different countries or regions. For example, studies in the British Derbyshire region (Dixon and Brook 2007), the Barcelonnette region of France (Jakob and Lambert 2009), Canada (Turkington et al. 2016), the Val d'Aranand region of Spain (Hürlimann et al. 2022), and China (Lin et al. 2020; Lin et al. 2022) have shown that climate change will lead to more frequent landslide occurrences and wider landslide impacts in the future. However, other researchers have conducted some landslide studies and shown that climate change will cause fewer landslides and slower movements in the future (Buma and Dehn 2000; Collison et al. 2000; Coe 2012; Rianna et al. 2014). In addition, some researchers have shown that the impacts of climate change on future landslides are uncertain or cannot be accurately assessed (Ciabatta et al. 2016; Alvioli et al. 2018). These works reveal significant regional differences and large uncertainties in studies of the impacts of climate change on landslides. Moreover, there is still insufficient research regarding how precipitation extremes under climate change scenarios influence landslides on a global scale.

A historical landslide casualty database provides a basis for projecting future casualties of landslides. At present, there are two types of global-scale landslide databases. One type includes data collected by national or international organizations such as the EM-DAT provided by the Centre for Research on the Epidemiology of Disasters (CRED) and the Global Landslide Catalog (GLC) database provided by the National Aeronautics and Space Administration (NASA). The other type comprises data collected and sorted by researchers. Froude and Petley (2018) established a 2004–2014 landslide disaster event database. Gómez et al. (2023) merged and depurated the EM-DAT, GLC, and the Disaster Inventory System (DesInventar) to obtain the Global Fatal Landslide Database (GFLD). However, due to the different data collection methods followed by different institutions and researchers, the collated landslide data differ. Some researchers have also tried to build models to assess the impacts of global or regional-scale landslide disasters on casualties. Nadim et al. (2006) considered the factors that influence landslides, including precipitation, lithology, topography, seismic activity, and soil moisture, to depict global landslide hazard "hot spots" by weighted stacking. Then, the "hot spot" results were combined with grid population of the world (GPW) provided by Columbia University to assess the global level of populations at risk of landslides. Yang et al. (2015) assessed the hazard of global landslides and then integrated the results with LandScan 2010 global population data to assess the global population at risk of landslides. Gariano et al. (2017) investigated the future variations in the impact of rainfall-induced landslides on the population of Calabria. They found a + 80.2% and + 54.5% increase in the impact on the population for the period 2036–2065, under the RCP4.5 and RCP8.5 scenarios, respectively. Emberson et al. (2020) estimated populations that were exposed to global landslides from 2001 to 2019 based on satellite precipitation data and the Landslide Hazard Assessment for Situational Awareness (LHASA) model. At present, existing global-scale assessment studies of populations at risk of landslides have not considered changes in future landslide risks of precipitation extremes under climate change scenarios.

In general, the annual average casualties caused by landslides are severe worldwide. However, the types, extents, locations, and frequencies of future landslides are still unclear under extreme precipitation change (Gariano and Guzzetti 2016), and this ambiguity will undoubtedly increase the difficulty and uncertainty associated with managing future landslide population risks. Therefore, this study used the Coupled Model Intercomparison Project (CMIP5) multi-downscaling General Circulation Models (GCM) daily precipitation data from the climate change Representative Concentration Pathway 4.5 (RCP4.5) scenario to project future changes in the frequency of extreme precipitation-triggered landslides and then combined future population data from the Shared Socioeconomic Pathway 2 (SSP2) scenario to assess the potential changes in global casualties of landslides in the future. The contributions of this study are the inclusion of extreme precipitation under climate change in the landslide risk assessment model and the realization of the quantitative assessment of future casualty risk of landslides induced by extreme precipitation.

## 2 Data and Method

The data used in this study contain global landslide and casualty data, influencing factors of landslide susceptibility, precipitation data, and population data. The research methodology includes the logistic regression model for landslide susceptibility, thresholds of extreme precipitation that triggers landslides, and population exposure and vulnerability calculations.

### 2.1 Data

The global landslide and casualty data provided by Lin et al. (2017), which combined two existing global landslide inventories—the World Geological Hazard Inventory created by the Academy of Disaster Reduction and Emergency Management of Beijing Normal University (ADREM, BNU),

**Table 1** Basic information of the 13 General Circulation Models (GCMs) used in this study

| Model/country | Model/country | Model/country |
|---|---|---|
| ACCESS1-0/Australia | CNRM-CM5/France | MIROC5/Japan |
| BCC-CSM1-1/China | GFDL-ESM2G/United States | MPI-ESM-MR/Germany |
| CanESM2/Canada | INMCM4/Russia | MRI-CGCM3/Japan |
| CCSM4/United States | IPSL-CM5A-LR/France | NorESM1-M/Norway |
| CESM1-BGC/United States | | |

and the global landslide inventory provided by NASA (see Kirschbaum et al. 2010 and Kirschbaum et al. 2015 for details). They used the time of the landslide occurrence as the crucial standard—when two landslide events occurred at different times (months), they were both included in the new database. If two events had the same occurrence time and their locations were close, investigation of details in the two landslide events could determine whether they were the same landslide. If that was the case, the record with the higher spatial resolution was included. This study selected the landslide events triggered by rainfall.

For the influencing factors of landslide susceptibility, this study considered lithology, slope, elevation, soil moisture, soil type, and vegetation cover based on the studies of Nadim et al. (2006), Hong et al. (2007), Nadim et al. (2013), Lin et al. (2017), Stanley and Kirschbaum (2017), and Lin and Wang. (2018). Since the spatial correlation between slope and elevation exceeds 0.38, slope was selected in this study, and elevation was excluded. After incorporating soil type data into the landslide susceptibility model, the model did not pass the significance test ($P > 0.1$) and thus soil type was excluded. Ultimately, slope, lithology, vegetation cover index, and soil moisture were chosen to construct a landslide susceptibility model. Slope data were from SRTM30, which is a global elevation dataset provided by NASA.[1] Lithology data were from the Geological Map of the World at 1/25,000,000 scale published by the Commission for the Geological Map of the World and UNESCO ($CGMW_{2000}$).[2] Vegetation cover index data are from the European Space Agency (Globcover 2000). Soil moisture data can be downloaded from the Internet[3] (Centre for Climatic research, University of Delaware).

Precipitation data were obtained from the Integrated MultisatellitE Retrievals for Global Precipitation Measurement (IMERG) data for 2000–2018 and the multi-GCM daily precipitation data for the historical (1971–2000) and future (2031–2060 and 2066–2095) periods derived from the NASA Earth Exchange-Global Daily Downscaled Projections (NEX-GDDP) dataset.[4] The GCM dataset provides daily precipitation data for 21 GCMs in the historical (1950–2005) and future (2006–2100) periods under the RCP4.5 and RCP8.5 scenarios (some models such as ACCESS1-0, bcc-csm1-1, and so on forecast daily precipitation for the future only up to 2095). This dataset has been indicated to be suitable for studies on climate change impact assessments in different regions of the world (Mandapaka and Lo. 2018; Lin et al. 2020). To reduce the redundancy and uncertainty resulting from the GCMs used in this study, the daily precipitation data of 13 GCMs (Table 1) from different institutions were selected (Zhang et al. 2021).

The global population data were obtained from Landscan-Oak Ridge National Laboratory (ORNL) in the United States[5] for 2000–2018 and the 1980–2100 population data from the SSP2 scenario published by the International Institute for Applied Systems Analysis (IIASA) in Austria.[6] The SSPs refer to the reference pathways of future socioeconomic development and were developed based on the RCPs; five scenarios are included: SSP1 (sustainability), SSP2 (middle of the road), SSP3 (regional rivalry), SSP4 (inequality), and SSP5 (fossil-fueled development) (O'Neill et al. 2014; O'Neill et al. 2017). Based on the RCP4.5 and RCP8.5 and SSP1–SSP5 scenarios, a 2×5 matrix can be generated. However, in some portfolios (such as SSP5-4.5, SSP1-8.5, and so on), these scenarios hardly emerge. Many existing studies selected data from the portfolios of SSP2-4.5 and SSP3-8.5, which have been widely compared and analyzed (Liu et al. 2020). The SSP2-4.5 scenario indicates moderate carbon emissions and moderate population growth, which is consistent with typical patterns of historical experience observed over the past century (O'Neill et al. 2017). In our study, the climate change SSP2-4.5 combined scenario was chosen to project landslide population risks. Detailed descriptions of these datasets are shown in Table 2.

[1] earthenv.org/topography

[2] https://ccgm.org/en/catalogue/

[3] https://climate.udel.edu/data/

[4] https://dataserver.nccs.nasa.gov/thredds/catalog/NEX-GDDP/

[5] https://landscan.ornl.gov/

[6] https://secure.iiasa.ac.at/web-apps/ene/SspDb/dsd?Action=htmlpage&page=about

**Table 2** Datasets involved in this study

| Dataset | Data content | Data source |
|---|---|---|
| Global landslide database | 8873 landslide[a] events | Lin et al. (2017) |
| Influencing factors of landslide susceptibility | Slope | earthenv.org/topography |
| | Lithology | https://ccgm.org/en/catalogue/ |
| | Soil moisture | https://climate.udel.edu/data/ |
| | Vegetation cover index | https://joint-research-centre.ec.europa.eu/scientific-tools-databases_en |
| Global precipitation data | Integrated MultisatellitE Retrievals for Global Precipitation Measurement (IMERG) | https://disc.gsfc.nasa.gov/datasets/ |
| | 13 GCMs from NASA Earth Exchange / Global Daily Downscaled Projections (NEX-GDDP) | https://www.nasa.gov/nex |
| Global population data | LandScan | https://landscan.ornl.gov/ |
| | SSP2 scenario | https://secure.iiasa.ac.at/web-apps/ene/SspDb/dsd?Action=htmlpage&page=about |

[a]Landslides in this study refer to landslide disasters in a broad sense, including slides, rockfalls, and debris flows (Hungr et al. 2014).

## 2.2 Method

Figure 1 shows the flowchart of this study. First, the logistic regression model was used to construct the landslide susceptibility model, and the accuracy of the model was validated and analyzed. Next, the annual average frequency of the 7-day antecedent rainfall index (ARI) exceeding the 95th percentile threshold (defined as the 95th percentile of ARI values for IMERG rainfall data from 2000–2014) was calculated for each grid globally from 2000–2018. The grids beyond the extreme precipitation threshold were combined with grids of very high, high, and moderate landslide susceptibility, and the average annual frequency of precipitation-triggered landslides was obtained. Then, the annual population exposure to landslides was calculated using the population data from LandScan for 2000–2018 and the results of precipitation-triggered landslides. The global landslide casualty data were used to calculate the average annual casualty rate on a national scale based on the annual population exposure to landslides.

Second, based on the historical (1971–2000) and future (2031–2060 and 2066–2095) rainfall data of multiple GCMs under the RCP4.5 scenario and the population data under the SSP2 scenario, the annual average population exposure (1971–2000, 2031–2060, and 2066–2095 under the SSP2-4.5 scenario) could be obtained by using the above calculation method. Then, this result was used to multiply the landslide disaster casualty rate to obtain the average annual landslide casualty risk for 1971–2000, 2031–2060, and 2066–2095 under the SSP2-4.5 scenario. It is important to note that, the global landslide casualty data (average annual casualty for 2000–2018 on a national scale) were used to correct the average annual casualty for 2000–2020 under the SSP2-4.5 scenario, and the result was used to correct the annual average landslide population risk on a national scale during the 1971–2000, 2031–2060, and 2066–2095 periods under the SSP2-4.5 scenario.

### 2.2.1 Logistic Regression Model

Logistic regression is a commonly used statistical analysis model for binomial categorical dependent variables and describes the relationship between the dependent variable (1 for occurrence and 0 for nonoccurrence) and multiple causal factors ($X_1$, $X_2$, ..., $X_i$). This model is commonly fitted in a stepwise manner (Budimir et al. 2015). The general form of a logistic regression model is:

$$P = \frac{\exp(\beta_0 + \beta_1 x_1 + \beta_2 x_2 + \cdots + \beta_i x_i)}{1 + \exp(\beta_0 + \beta_1 x_1 + \beta_2 x_2 + \cdots + \beta_i x_i)} \quad (1)$$

where $P$ is the probability of landslides, $\beta_0$ is a constant, $x_1$ ,$x_2$, …,$x_i$ are the independent variables related to the explanatory factors, $\beta_1$,$\beta_2$, …,$\beta_i$ are the regression coefficients for the explanatory factors.

Data from landslide sites (8873) and randomly generated landslide nonoccurrence sites (8700) were included as independent variables in the model (1 for landslide occurrence and 0 for nonoccurrence of landslide). The landslide nonoccurrence sites were generated from the global non-landslide susceptibility map (Jia et al. 2021), which provides locations where the global likelihood of landslide occurrence is null or negligible. Slope, lithology, ground motion, land use type, and soil moisture were selected to construct the global landslide susceptibility. The highest

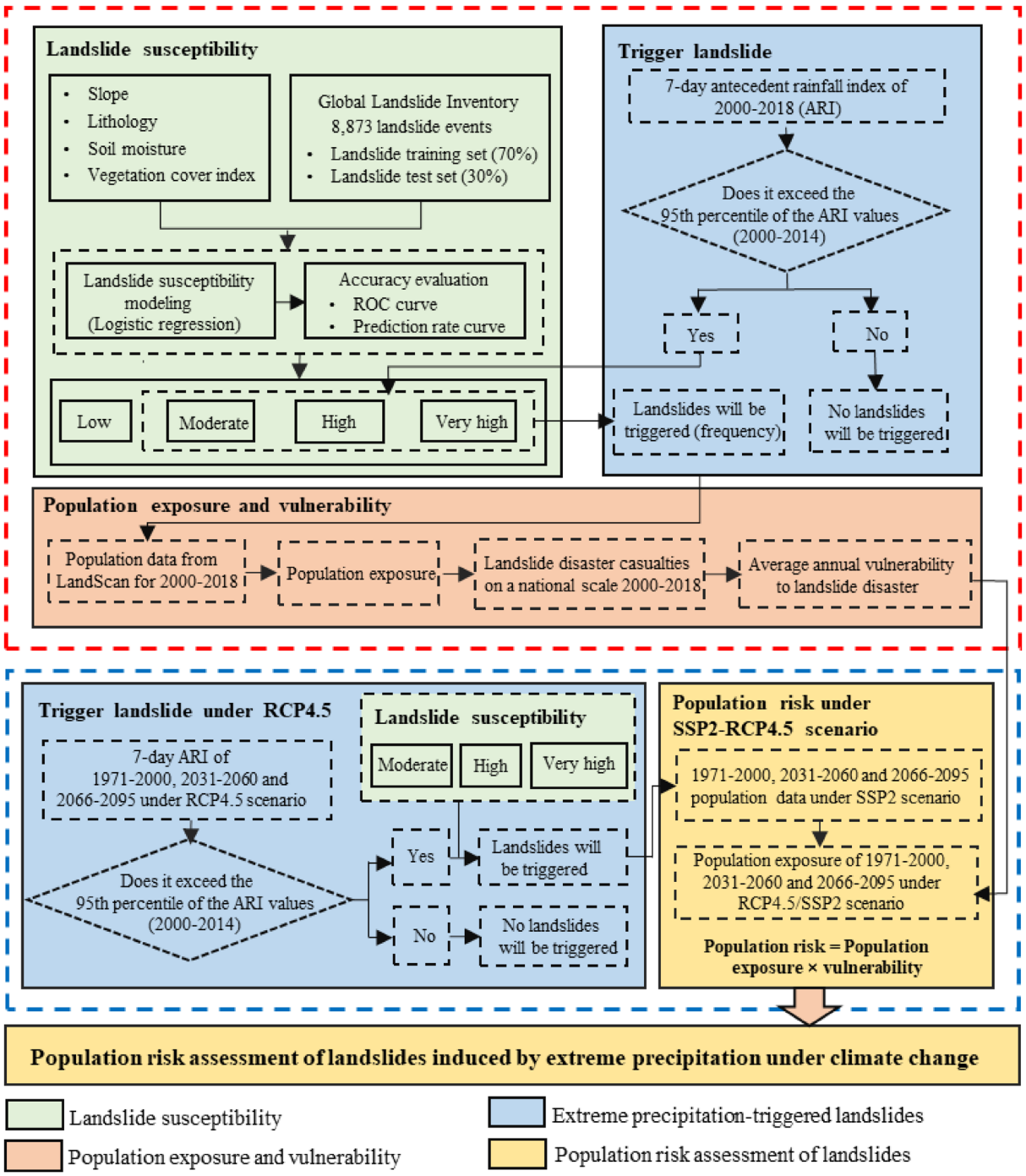


**Fig. 1** Flowchart of the landslide casualty risk assessment of precipitation extremes under a climate change scenario in this study. ARI = Antecedent rainfall index.

grid resolution of data available for this study was 1 km, so the influencing factors of landslides were resampled to 1 km in Arcgis 10.6 in accordance with the proximity principle. In this study, 70% of data from randomly selected landslide and non-landslide samples were used as training samples and substituted into the logistic regression model. Detailed descriptions and processes of these datasets are shown in Table 3.

### 2.2.2 Extreme Precipitation that Triggers Landslides

Extreme precipitation is an important factor in triggering landslides. Since there are significant differences in extreme

**Table 3** Input variables used in the logistic regression analysis

| Dependent variable: landslide location | Map details |
|---|---|
| Global Landslide sites | Point data |
| Independent variables: | Map details |
| **Slope**<br>Classification method: refer to Nadim et al. (2006)<br>(1. 0°–1°; 2. 1°–8°; 3. 8°–16°; 4. 16°–32°; 5. > 32°) | 1 km |
| **Lithology**<br>Classification method: see Nadim et al. (2006)<br>(0. Undifferentiated facies, Ophiolitic complex, Endogenous rocks, Oceanic crust; 1. Extrusive volcanic rocks: Precambrian, Proterozoic, Paleozoic and Archean; Endogenous rocks (plutonic and/metamorphic): Precambrian, Proterozoic, Paleo Archean; 2. Old sedimentary rocks: Precambrian, Archean, Proterozoic, Paleozoic; Extrusive volcanic rocks: Paleozoic, Mesozoic; Endogenous rocks: Paleozoic, Mesozoic, Triassic, Jurassic, Cretaceous; 3. Sedimentary rocks: Paleozoic, Mesozoic, Triassic, Jurassic, Cretaceous; Extrusive volcanic rocks: Mesozoic, Triassic, Jurassic, Cretaceous; Endogenous rocks: Meso-Cenozoic, Cenozoic; 4. Sedimentary rocks: Cenozoic, Quaternary; Extrusive volcanic rocks: Meso-Cenozoic; 5. Extrusive volcanic rocks: Cenozoic) | Polygon (rasterized into 1 km) |
| **Soil moisture index**<br>Classification method: see Nadim et al. (2006)<br>(1. -1.0 to -0.6; 2. -0.6 to -0.2; 3. -0.2 to 0.2; 4. 0.2 to 0.6; 5. 0.6 to 1.0) | 5 km (rasterized into 1 km) |
| **Vegetation cover index**<br>Classification method: see Jaedicke et al. (2014)<br>(0. Water; 1. Urban; 2. Forest; 3. Grassland; 4. Farmland; 5. Bare surface) | 1 km |

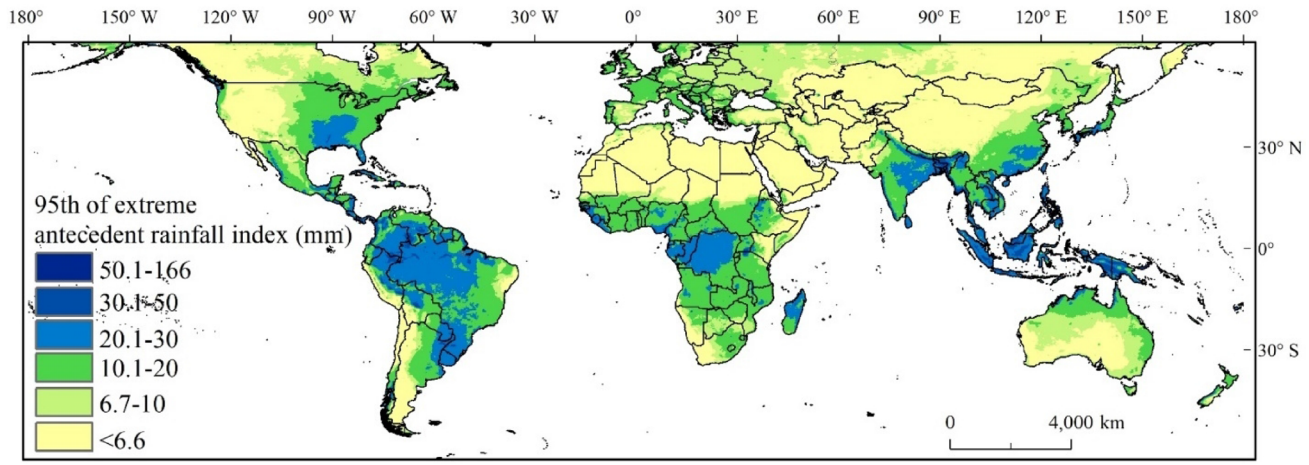


**Fig. 2** Global 95th percentile of the extreme antecedent rainfall index (ARI). *Source* Kirschbaum and Stanley (2018).

precipitation conditions in different climatic zones globally, the extreme precipitation thresholds for triggering landslides should take into account regional variability. There have been many different treatments on how to represent the landslide-triggering rainfall threshold (Caine 1980; Piciullo et al. 2018; Guzzetti et al. 2020). Kirschbaum and Stanley (2018) used continuous daily precipitation data from IMERG (2000–2014) to calculate precipitation for multiple time windows using a weighted index for each grid and assigned an extreme threshold to each grid using the 95th percentile of the ARI (Fig. 2). Then, using 949 global landslide events from 2007 to 2013, Kirschbaum et al. (2015) validated the results of the established extreme ARI thresholds for triggered landslides over multiple time windows using the results of global landslide susceptibility and found the best validation results using a 7-day window and a weighted exponent of -2. In some very dry areas, the 95th percentile ARI is still low. In order to avoid erroneous predictions in desert regions, Kirschbaum and Stanley (2018) adopted a conservative minimum ARI threshold of 6.6 mm. They validated their global 7-day weighted ARI extreme precipitation threshold for landslide-triggering by using the 4930 rainfall-induced landslides that have occurred in the GLC, and the result shows that there were about 30% true positive rates (TPR) for induced landslides in areas of moderate and high susceptibility, and 40% TPR for induced landslides in

the Nepal landslides database established by Petley et al. (2007). The extreme precipitation thresholds for triggering landslides on a global scale constructed by Kirschbaum and Stanley have proved to be applicable, which is detailed in Kirschbaum and Stanley (2018). It is important to emphasize that the 7-day weighted ARI extreme precipitation-induced landslides are mainly shallow and intermediate landslides. The specific equation of ARI is:

$$\mathrm{ARI} = \frac{\sum_{t=0}^{6} P_t w_t}{\sum_{t=0}^{6} w_t} \tag{2}$$

where $t$ is the number of days before the present, $P_t$ is the precipitation at time $t$, and $W_t = (t+1)^{-2}$.

Annual frequencies of 7-day weighted ARI values exceeding the 95th percentile were calculated for IMERG 2000–2018, the NEX-GDDP historical period (1971–2000), and future periods (2031–2060 and 2066–2095) under the RCP4.5 scenario. The spatial resolutions of the IMERG daily precipitation and NEX-GDDP daily precipitation data are 1 km and 25 km, respectively, and the NEX-GDDP daily precipitation data spatial resolution was increased using proximity sampling to be consistent with the global landslide susceptibility (1 km):

$$F_v = \mathrm{ARI}_i - \mathrm{ARI}_{95\mathrm{th}} \tag{3}$$

where $F_v$ is the annual frequency of 7-day weighted ARI values above the 95th percentile weighted ARI, and $\mathrm{ARI}_i$ is the 7-day weighted ARI value for IMERG 2000–2018, the NEX-GDDP historical (1971–2000) and future (2031–2060 and 2066–2095) periods, $i = 1, 2, \ldots, 30$. The $\mathrm{ARI}_{95\mathrm{th}}$ is the 95th percentile 7-day weighted ARI values during IMERG 2000–2014. The annual frequency of landslide disasters triggered by extreme precipitation at each grid (1 km×1 km) was obtained when 7-day weighted ARI values exceeded the 95th percentile extreme threshold and was overlaid with a very high, high, and moderate landslide susceptibility grid.

#### 2.2.3 Population Exposure and Population Vulnerability

Landslide population exposure is closely related to landslide susceptibility. According to Jaedicke et al. (2014), Eq. 4 was used to calculate the landslides population exposure corresponding to different landslide susceptibility classes (Jaedicke et al. used this method to calculate the population exposed to landslides in Europe and further obtained the population risk, and the method was validated based on the actual landslide casualties, showing that the model works well). By combining these results with the annual frequency of landslides triggered by extreme precipitation in Sect. 3.2, the annual population exposure to landslides was obtained. Since the 95th percentile precipitation threshold for triggering landslides covers 60°N–60°S (Kirschbaum and Stanley 2018), the population exposure for extreme precipitation-triggered landslides also covers countries at 60°N–60°S, with the population exposure to landslides in the northern parts of some countries, such as northern Canada and northern Russia, not included. Referring to Emberson et al. (2020), the population exposure to landslides calculated in this study is the total exposed population impacted by the annual number of landslides triggered by extreme precipitation:

$$P_{\mathrm{Exp}} = \text{Very high} \times 1 + \text{high} \times 0.3 + \text{moderate} \times 0.1 + \text{low} \times 0 \tag{4}$$

where $P_{\mathrm{Exp}}$ is the population exposure to landslides and very high, high, moderate, and low represent the landslide susceptibility classes.

As the exposed populations obtained above are grid results (a combination of grids exceeding extreme precipitation thresholds and grids with very high, high, and moderate susceptibility to landslides), the exposed populations at the grid scale need to be summed to the national scale. The annual average population vulnerability to landslides on a national scale was calculated using the landslide casualty data from 2000–2018 in the global landslide database (the catastrophic landslide events north of 60°N were excluded to be consistent with the extent of population exposure to landslides) and Eq. 5. The spatial resolutions of the population data in the Landscan and SSP2 are 1 km and 5 km, respectively, and the SSP2 scenario population was resampled to 1 km using the average distribution method in Arcgis10.6 in accordance with the proximity principle:

$$\mathrm{Vul} = K / P_{\mathrm{Exp}} \tag{5}$$

where Vul is the landslides vulnerability on a national scale, and $K$ is the casualties caused by landslides on the same scale.

#### 2.2.4 Casualty Risk Assessment

According to Eq. 6, the risk of future casualties from landslides under climate change scenarios can be realized. It should be emphasized that the daily precipitation data for 13 GCMs under the RCP4.5 scenario and projected future population data under the SSP2 scenario deviate from actual future precipitation and population data, thus the assessed future landslide casualty risk deviates from the actual future scenario. To reduce this bias, the collected casualty data for 96 countries during 2000–2018 were used to revise the average annual casualty risk to landslides during the same period under the SSP2-4.5 scenario on a national scale. Then, the revised value in different countries was used to revise the landslide casualty

**Table 4** Modeling results of the logistic regression for landslide susceptibility

| Modeling (70%) | | | | | Validation (30%) | | | | |
|---|---|---|---|---|---|---|---|---|---|
| | | Projection of landslides | | Percent correct | | | Projection of landslides | | Percent correct |
| | | Yes | No | | | | Yes | No | |
| Actual landslides | Yes | **4298** | 1913 | 69.2% | Actual landslides | Yes | **1939** | 723 | 72.8% |
| | No | 1849 | **4241** | 69.6% | | No | 803 | **1807** | 69.2% |

risk during the 1971–2000, 2031–2060, and 2066–2095 periods under the SSP2-4.5 scenario:

$$K_{\mathrm{Fut}} = \mathrm{Vul} \times P_{\mathrm{Fut-Exp}} \tag{6}$$

where $K_{\mathrm{Fut}}$ is the future landslide casualties under the SSP2-4.5 scenario on a national scale, and $P_{\mathrm{Fut\text{-}Exp}}$ is the future population exposure to landslides.

## 3 Results

Using the above data and methods, the study obtained the spatial distribution of global landslide susceptibility, landslide population exposure and vulnerability, changes in landslide frequency due to extreme precipitation under the climate change RCP4.5 scenario, and prediction of landslide casualty risk under the SSP2-4.5 scenario.

### 3.1 Global Landslide Susceptibility

The results of the logistic regression model are shown in Eq. 6. The validation results of the logistic regression model are shown in Table 4. Bold text indicates landslides and non-landslides that were correctly simulated by the logistic regression model. In the 70% training set, the percentage of correct predictions for landslides was 69.2%, in the 30% validation set, the percentage of correct predictions was 72.8% and the area under the ROC curve (AUC) value of the model was 0.71, and the value of each influencing factor passed the significance test ($p < 0.05$). The accuracy of the logistic regression model was reasonable:

$$P = \frac{\mathrm{Exp}(-0.323 + 0.516 * S + 0.035 * L - 0.428 * VC + 0.164 * SM)}{1 + \mathrm{Exp}(-0.323 + 0.516 * S + 0.035 * L - 0.428 * VC + 0.164 * SM)} \tag{6}$$

where $P$ is the probability of landslides, and $S$, $L$, $VC$, and $SM$ represent the landslide explanatory factors of slope, lithology, vegetation cover index, and soil moisture, respectively.

The factors influencing landslide susceptibility were brought into Eq. 6 to obtain global landslide susceptibility. Based on the principle of logistic regression models (where landslides are likely to occur when the probability value is $> 0.5$), and using natural breaks in Arcgis10.6 to classify landslide susceptibility, the results identify the four levels with segmentation points of 0.5, 0.66, and 0.79 to predict the occurrence of landslides. As shown in Fig. 3 (the grid size is 1 km × 1 km), areas with very high landslide susceptibility are mainly distributed in the Cordillera in North America and South America, the Alps and Scandinavia in Europe, and the Himalayas, the northern Mongolian plateau, and the Malay Archipelago in Asia.

### 3.2 Global Landslide Population Exposure and Vulnerability

Figure 4 shows the average annual population exposure and vulnerability to landslides on a national scale from 2000–2018. The population exposure to landslides is mainly distributed in Mexico in Central America, and Pakistan, India, China, Indonesia, and Japan in Asia. Among the 96 countries considered, 24% had a landslide vulnerability of over 1 casualty per million people, which means one casualty for every one million exposure population to landslides, and 47% of the countries had a landslide vulnerability between 0.1 and 1 ppm. The top 10 countries with the highest annual average vulnerability to landslides, as measured by casualties per million people, are Côte d'Ivoire (18.4), Rwanda (6.8), Uganda (5.6), Burundi (5.2), Haiti (5), Brazil (4.2), Jamaica (3.2), the Philippines (3), Turkey (2.8), and China (2.4). For the average annual casualties from landslides collected from 2000–2018, the 10 highest countries were China, India, the Philippines, Indonesia, Turkey, Rwanda, Afghanistan, Brazil, Nepal, and Colombia, all of which had 120 or more casualties. Some of these countries have a wide distribution of mountainous areas (China, India, Nepal, Turkey), or are affected by extreme precipitation (Indonesia, the Philippines, Brazil), causing the average annual frequency and casualty rate of landslides to be high.

**Table 5** Top 20 countries with high landslide population risk during the 1971–2000, 2031–2060, and 2066–2095 periods and change from the 1971–2000 level under the SSP2-4.5 scenario

| Country | 1971–2000 | 2031–2060 | | 2066–2095 | |
|---|---|---|---|---|---|
| | Casualties | Casualties | Change (%) | Casualties | Change (%) |
| China | 1070 | 1670 | 56 | 1160 | 8 |
| India | 360 | 760 | 111 | 690 | 92 |
| Turkey | 220 | 450 | 104 | 420 | 91 |
| Philippines | 170 | 470 | 176 | 690 | 265 |
| Indonesia | 160 | 380 | 137 | 370 | 131 |
| Afghanistan | 150 | 630 | 320 | 880 | 487 |
| Brazil | 140 | 200 | 43 | 230 | 64 |
| Rwanda | 130 | 520 | 300 | 790 | 508 |
| Nepal | 100 | 260 | 160 | 290 | 190 |
| Guatemala | 70 | 150 | 114 | 180 | 157 |
| Colombia | 60 | 140 | 133 | 150 | 150 |
| Myanmar | 50 | 120 | 140 | 110 | 10 |
| Pakistan | 50 | 110 | 120 | 80 | 60 |
| Ethiopia | 40 | 100 | 150 | 130 | 225 |
| Peru | 40 | 60 | 50 | 50 | 25 |
| Uganda | 30 | 140 | 367 | 180 | 500 |
| Bangladesh | 20 | 120 | 500 | 130 | 550 |
| Burundi | 20 | 60 | 200 | 50 | 150 |
| Vietnam | 10 | 60 | 500 | 90 | 800 |
| Yemen | 10 | 50 | 400 | 90 | 800 |

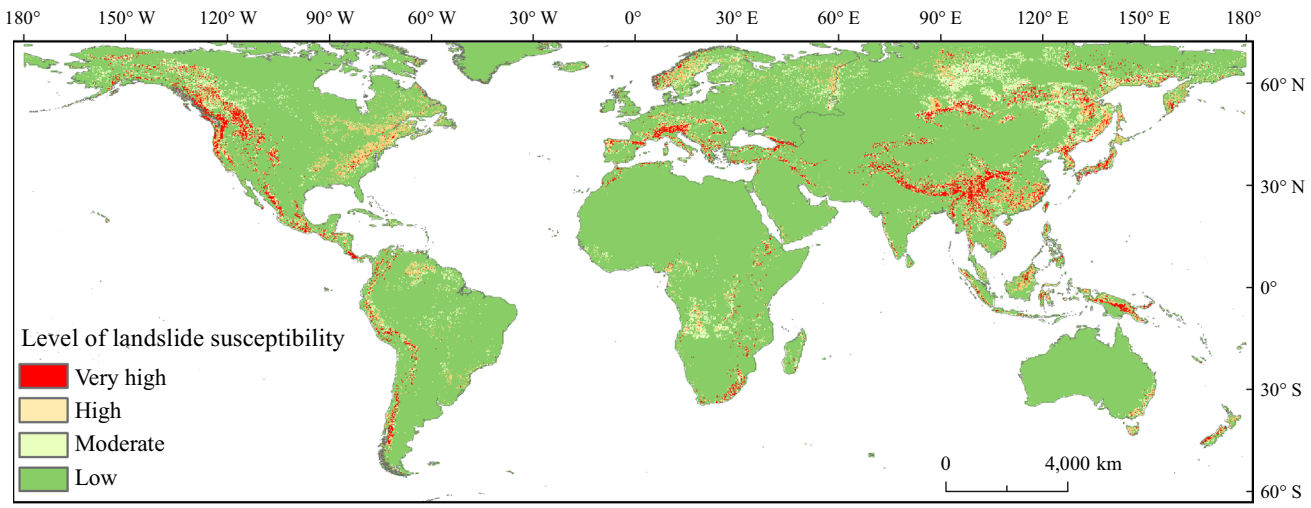


**Fig. 3** Spatial distribution of global landslide susceptibility

### 3.3 Change in the Frequency of Landslides Triggered by Extreme Precipitation under the Climate Change RCP4.5 Scenario

Figure 5 shows the change in the frequency of extreme precipitation-triggered landslides in 2031–2060 and 2066–2095 compared to 1971–2000. Under the climate change RCP4.5 scenario, the increase in extreme precipitation in the future is projected to trigger more landslides, and the increase is projected to be more significant in the late twenty-first century than in the mid-twenty-first century. Compared to the 1971–2000 period the average annual frequency of landslides increases by 7% and 10% during the 2031–2060 and 2066–2095 periods, respectively. Asia and Africa have the most significant change in rainfall-induced landslides, with 13% and 20% increases, respectively, in 2066–2095. The regions where the average annual frequency of landslides will increase most significantly are the northwestern side

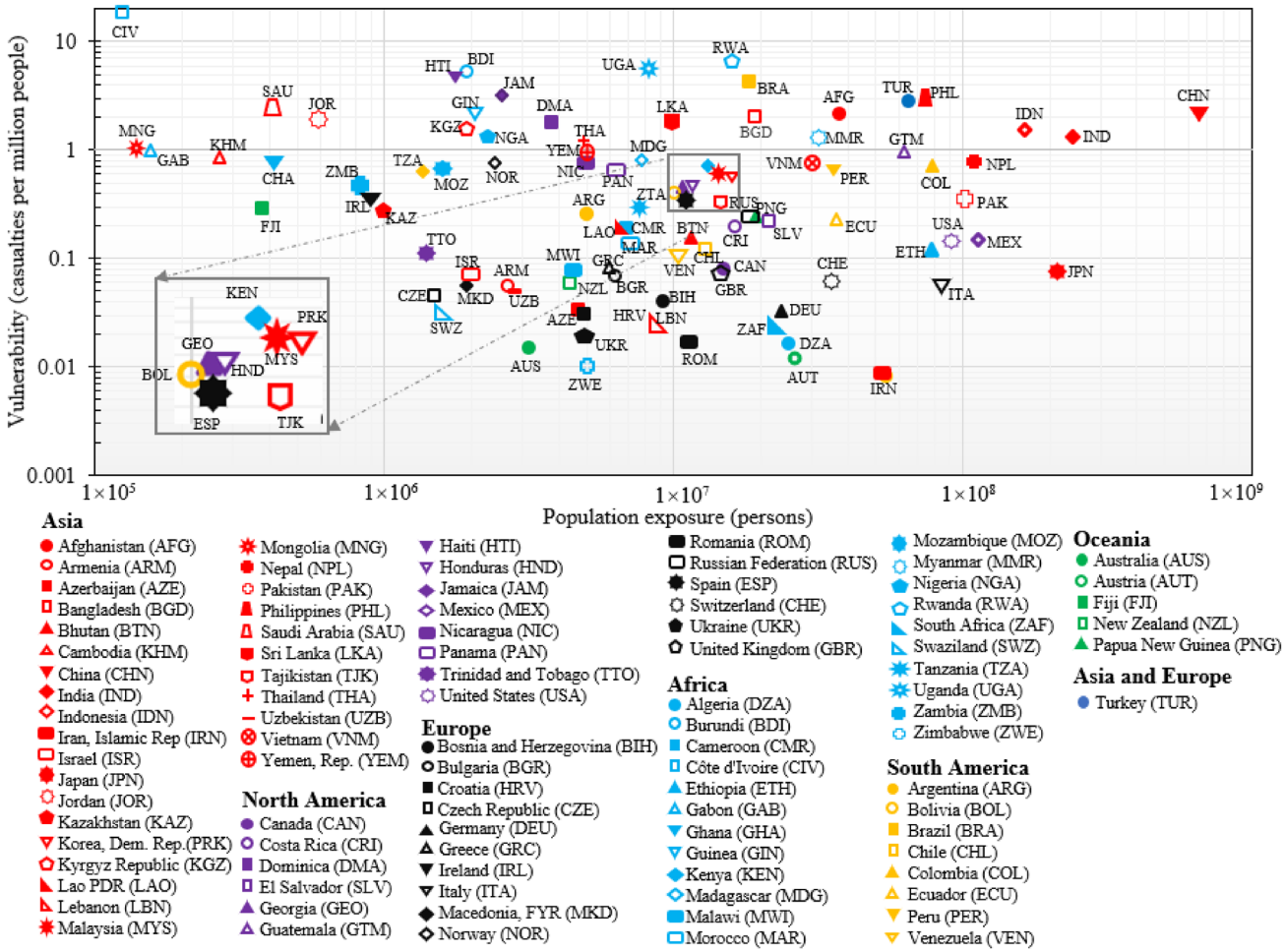


**Fig. 4** Average annual population exposure and vulnerability to landslides on a national scale, 2000–2018 (country name abbreviations used the International Standards Organization (ISO) 3-digit alphabetic codes)

of the Andes, the Hengduan Mountains in China, and the Malay Archipelago, which will have serious implications for future population risk in these regions.

### 3.4 Projection of Landslide Casualty Risk under the SSP2-4.5 Scenario

The results showed that the average annual casualty risk caused by landslides was projected to increase from 3240 during the 1971–2000 period to 7670 and 8380 during the 2031–2060 and 2066–2095 periods, and the growth rates will be 140% and 160%, respectively, under the SSP2-4.5 scenario. The top 20 countries with high landslide population risks (cumulatively account for more than 85% of the risk in the 96 countries) are shown in Table 5. The average annual casualties due to landslides in Asian countries are consistently high, particularly the estimated number of landslide casualties in China (1670), India (760), Afghanistan (630), the Philippines (470), and Indonesia (380) during the 2031–2060 period under the SSP2-4.5 scenario. Compared to the 1971–2000 period, Asia has the most significant increase in annual average casualties of landslides in the mid- and late twenty-first century. Among them, the average annual casualties in the above countries increased by more than 200 during the 2031–2060 period under the SSP2-4.5 scenario. The reason is that changes in the future population scale play an important role, with China, India, and Indonesia projected to be the most populous countries, which are also located in high-risk landslide areas, causing the casualties of landslides to be the most significant. Compared to 1971–2000, Bangladesh, Vietnam, and Yemen show higher change in landslide casualties, and the numbers in all of these countries exceed 500% during the 2066–2095 period, so these countries belong to potentially high casualty risk countries. In the future, countries with high casualties and high growth rates should further strengthen their disaster warning and management capabilities to reduce the population losses resulting from landslides.

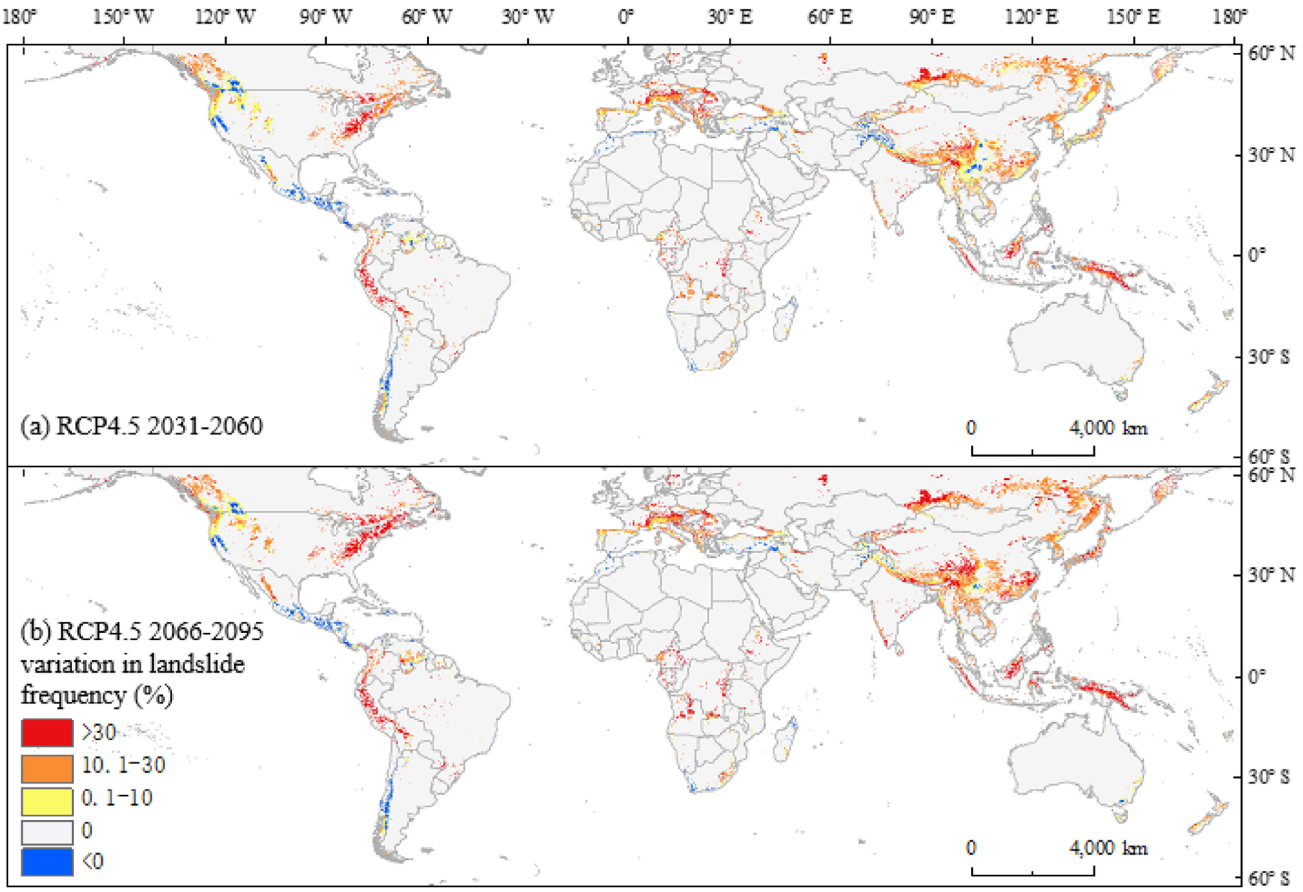


**Fig. 5** Changes in the average annual frequency of extreme precipitation-triggered landslides under the RCP4.5 scenario (ensemble average of multiple models) in 2031–2060 and 2066–2095 compared to 1971–2000

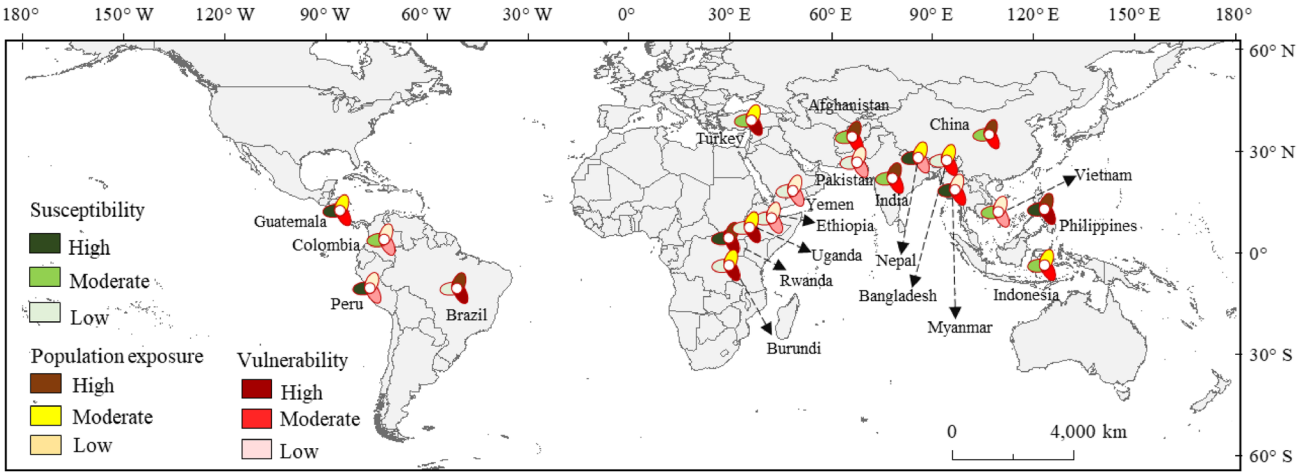


**Fig. 6** The impact of landslide susceptibility, exposed population, and vulnerability on landslide casualty risk during the 2066–2095 period under the SSP2-4.5 scenario

Figure 6 shows the impact of landslide susceptibility, population exposure, and vulnerability on the top 20 countries with high casualty risk to landslides during the 2066–2095 period under the SSP2-4.5 scenario. Each impact factor (landslide susceptibility, population exposure, and vulnerability) value for the 20 countries was ranked, with

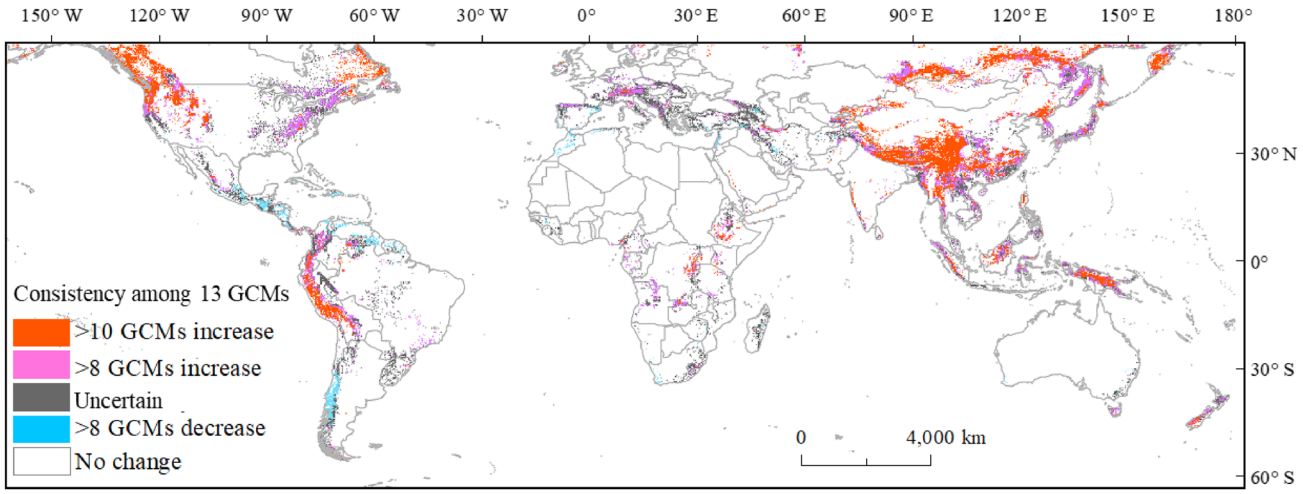


**Fig. 7** 13 General Circulation Model (GCM) consistency of change in annual average landslide frequency during the 2066–2095 period compared with that during the 1971–2000 period under the RCP4.5 scenario

the top 1–6 countries classified as having a high impact, those ranked 7–13 as having a medium impact, and those ranked 14–20 as having a low impact. High susceptibility to landslides has a significant impact on casualties in Nepal, Guatemala, Myanmar, and Peru, and all of these countries have a probability of landslide susceptibility exceeding 0.75. The high casualty risk of future landslides in China, Afghanistan, and India is mainly due to the high population exposure to landslides, and in all of these countries the total number of repeatedly exposed population exceeds 970 million per year. Countries such as Uganda, Turkey, and Burundi are more likely to be affected by high vulnerability to landslide disasters (more than 2.8 casualties per million people). The high casualty risk in Brazil is affected by both a highly exposed population and a high vulnerability to landslides. The Philippines and Rwanda are affected by high landslide vulnerability, high population exposure, and high vulnerability to landslides.

## 4 Discussion

In the reports published by the IPCC Working Group II in 2007 (Parry et al. 2007) and 2014 (Barros et al. 2014), the issues of local and regional landslides were specifically mentioned, but no overview of global landslides was included. This study incorporates extreme precipitation under climate change scenarios into a landslide risk assessment model, enabling a quantitative assessment of future global casualty risk. This section discusses the uncertainty, the contribution of our study compared to previous studies, and the advantages/disadvantages of the used study approaches.

### 4.1 Uncertainty Analysis

Based on the study of historical short-period landslide susceptibility, this study projected the change in the annual frequency of landslides triggered by extreme precipitation during the 2031–2060 and 2066–2095 periods under the RCP4.5 scenario compared with that during the 1971–2000 period. The daily precipitation data from the 13 GCMs from different institutions with simulated variations in extreme precipitation are projected to have an increasing trend in the future, for which the most significant increase is near the equator (Malay Archipelago) and in southern China. According to Sooraj et al. (2015), the Asian summer monsoon will have a more intense impact on the Malay Archipelago and southern China in the future, leading to an increase in precipitation. As a result, the predicted frequency of landslides triggered by extreme precipitation also has an increasing trend. However, due to uncertainties in climate model precipitation data (imperfections in climate models, uncertainties in emission scenarios, differences in downscaling methods), the results of global climate simulations conducted by different institutions vary (Crozier 2010; Melchiorre and Frattini 2012; Villani et al. 2015). As shown in Table 6, compared with the 1971–2000 period, the 2066–2095 period demonstrates changes in landslide frequency ranging from 5% (CanESM2) to 15% (ACCESS1-0), the bold text indicates the ensemble average changes in landslide frequency of the 13 models. Figure 7 shows the consistency of change in the modeling results of annual average landslide frequency triggered by extreme precipitation during the 2066–2095 period compared with that during

**Table 6** Change in landslide frequency during the 2031–2060 and 2066–2095 periods compared with that during the 1971–2000 period under the RCP4.5 scenario (%)

| General circulation model (GCM) | 2031–2060 | 2066–2095 | General circulation model (GCM) | 2031–2060 | 2066–2095 |
|---|---|---|---|---|---|
| Ensemble average of multimodel | **7** | **10** | CFDL-ESM2G | 6 | 8 |
| ACCESS1-0 | 12 | 15 | INMCM4 | 2 | 7 |
| BCC-CSM1-1 | 5 | 9 | IPSL-CM5A-LR | 12 | 14 |
| CanESM2 | 5 | 5 | MIROC5 | 14 | 14 |
| CCSM4 | 4 | 7 | MPI-ESM-MR | 5 | 6 |
| CESM1-BGC | 6 | 12 | MRI-CGCM3 | 5 | 6 |
| CNRM-CM5 | 4 | 7 | NorESM1-M | 11 | 15 |

the 1971–2000 period under the RCP4.5 scenario. The 13 models showed a reasonable degree of consistency in their projected increases and decreases—in Fig. 7, regions with more than 10 of these models showing an increase in the projected values occupy the largest area, and are mainly distributed in northwestern North America and northwestern South America, the Himalayas, and northern Asia; regions with more than 8 models showing an increase in the projected values have a much smaller area, and are mainly distributed in northeastern North America and Europe; while regions with more than 8 models showing a decrease are small in area, and are mainly distributed in Central America and southwestern South America, and regions with roughly equal number of models showing an increase and a decrease ("uncertain") spread broadly. Table 6 and Fig. 7 illustrate that using only a single GCM to project the future casualties caused by landslides under the climate change scenario results in some uncertainties. The ensemble average of the projection results of multiple models can be used to reduce the uncertainty caused by a single GCM to a certain extent.

The accuracy of hourly precipitation-induced landslides will be higher than that of daily precipitation—for example, when persistent heavy precipitation occurs, more than one landslide event may occur at the same landslide site in a day (Ma et al. 2023), thus using daily precipitation may underestimate the frequency of extreme precipitation-induced landslides. However, for the current predicted precipitation from general circulation models, the spatial resolution of hourly precipitation is coarse, usually 50 km, and cannot be applied to the analysis of landslides induced by extreme precipitation globally. Therefore, the daily precipitation data from the GDDP provided by NASA were used in this study. The analysis of future landslide frequency change compared to the historical period can reduce some errors.

The casualty rate for landslides was calculated based on historical landslide casualty data, which is the main basis for projecting future population risks to landslides (Emberson et al. 2020). The existing global landslide databases (Petley 2012; Lin et al. 2017; Farahmand and AghaKouchak 2013) are based on major landslide events, and the records of small, noncatastrophic landslide events are generally lacking; in addition, there is a lack of casualty records of landslides triggered by earthquakes and tropical cyclones, for example, the 8.0 magnitude Wenchuan Earthquake in China in 2008, which triggered landslides that caused more than 10,000 casualties, and the 1998 landslide triggered by Hurricane Mitch at the Casita volcano in Nicaragua, which killed more than 2500 people—this inevitably leads to underestimations of the casualty rate for landslides. More work needs to be done in the future to improve the quantity, quality, and integrity of global landslide databases (Van Den Eeckhaut and Hervás 2012). Therefore, the relative change of future landslide casualties obtained in this study is more representative. Due to the uncertainties inherent in multiple climate models, there is also some variation in the change of casualty risk based on different models (Fig. 8). In the 13 GCMs, compared to 1971–2000, the ACCESS1-0 model simulated a higher increase rate in casualties of extreme rainfall-induced landslides, and the CanESM2 model simulated a lower increase rate during 2066–2095 under the SSP2-4.5 scenario. Within the 95% confidence interval, Afghanistan, Nepal, Pakistan, and Uganda have the highest confidence levels (Fig. 8). This means that the 13 GCMs simulated casualty risk for these countries with less variability, while other countries have larger confidence intervals, exceeding the allowable margin of error, showing larger differences in the assessed results by different models.

## 4.2 Contribution and Limitations of this Study

In the modeled global landslide susceptibility, it was found that the very high landslide susceptibility areas are mainly distributed in the Cordillera in North America and South America, the Alps and Scandinavia in Europe, and the Himalayas, the northern Mongolian plateau, and the Malay Archipelago in Asia. This distribution is generally consistent with the spatial distribution of global high landslide

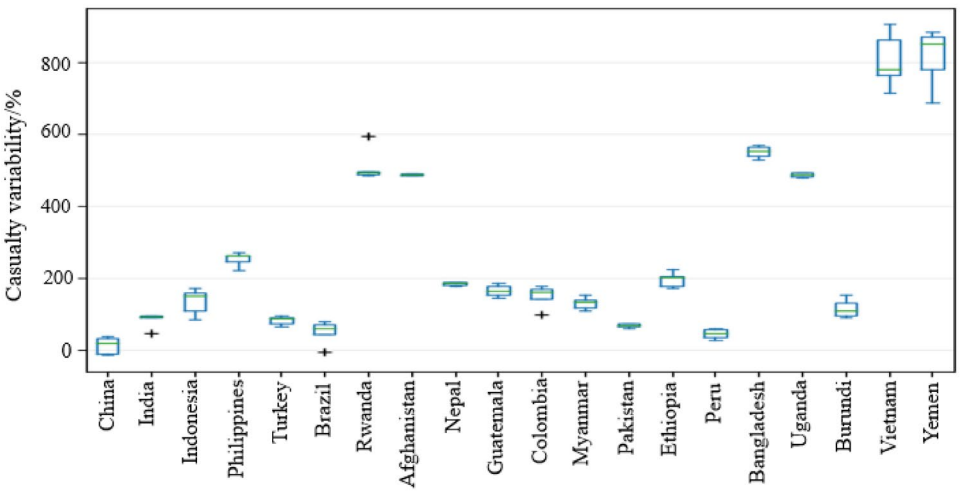


**Fig. 8** Variability of projected change in the casualties of landslides at the end of the twenty-first century under the SSP2-4.5 scenario compared to 1971–2000 for the top 20 countries with high casualty risk based on the 13 General Circulation Models (GCMs)

susceptibility areas obtained by Nadim et al. (2006), Hong et al. (2007), Farahmand and AghaKouchak (2013), Stanley and Kirschbaum (2017), and Lin et al. (2017). The progress of this study was that in the construction of the landslide susceptibility model, the landslide nonoccurrence sites were generated from the global non-landslide susceptibility map of Jia et al. (2021), and this study used the World Geological Hazard Inventory provided by ADREM of BNU and the global landslide inventory provided by NASA—the two largest global inventories of landslides (Lin et al. 2017) for the modeling and validation of global landslide susceptibility, which further improves the accuracy of the model.

Based on the examination of global landslide susceptibility distribution, this study used extreme precipitation to analyze landslide frequencies (Kirschbaum and Stanley2018). Compared with previous studies, this study coupled 13 GCM precipitation datasets of the CMIP5 under the climate change RCP4.5 scenario to obtain the spatial and temporal distribution of the global landslide frequency induced by extreme rainfall in the future. Furthermore, this study obtained the frequency of future landslides induced by extreme rainfall globally compared to the historical period, which is beneficial to the countries with high landslide occurrences to reduce the landslide hazards in the future. The occurrence of landslides poses serious threats to local populations. Published studies on landslide impacts on populations have focused on exposed populations (Gariano et al. 2017; Emberson et al. 2020) or at-risk population assessments at regional scales (Rong et al. 2023). This study further incorporates future population data from the SSP2 scenario into the landslide population risk assessment model to achieve future landslide casualty assessment at a global scale.

The projection of casualty risk of landslides was based on daily precipitation data under the climate change RCP4.5 scenario and population data under the SSP2 scenario, both of which have some inherent uncertainties. Although multi-GCMs were used to reduce these uncertainties and nationwide casualty data were used to reduce the biases in the population risk assessment results, due to the relatively local impacts of landslides and the lack of a global monitoring network for landslides similar to those that exist for earthquakes and typhoons, landslide databases are often difficult to obtain. This scarcity results in limited global-scale assessments of casualty risk of landslides. In addition, this study was based on a constant vulnerability index to assess future casualties of landslides, but with the socioeconomic development, many countries have better landslide early warning equipment, knowledge of disaster avoidance, and medical aid equipment, such as some European countries located in and around the Alps (Italy, France, and Germany), which will reduce the population vulnerability to landslides to a certain extent (Pecoraro et al. 2019). Although it is still difficult to quantify future landslide population vulnerability, more work is needed to anticipate the impact of economic and social development on landslide population vulnerability. This study examined trend in a statistical sense, with the aim of incorporating precipitation data under climate change scenarios into the landslide risk assessment model to project the trends of future extreme precipitation-triggered landslide casualty risk on a global scale. The latest CMIP6 general circulation model was not used in this study due to its relatively low resolution (0.5 degrees) compared to the one used in this study (0.25 degrees). In future studies, we will introduce more new models to reduce the uncertainty. Accurate predictions of populations at risk of landslide disasters also require more scientific spatial downscaling of climate model data in small-scale regions and the collection of more complete landslide casualty data.

## 5 Conclusion

In this study, based on the spatial distribution of global landslide susceptibility, an input module including precipitation data from multi-GCMs projected under the RCP4.5 scenario was added to the landslide population risk assessment model. Based on the global landslide databases, this study calculated the annual average landslide casualty rate from 2000–2018 on a national scale. On this basis, it also projected the risks of future populations from landslides using multi-GCMs under the SSP2-4.5 scenario. The main results are as follows:

(1) Under the RCP4.5 climate change scenario, the change in the annual frequency of landslides triggered by extreme precipitation is predicted to increase globally. Compared to the 1971–2000 period, the average annual frequency of landslide hazards increases by 7% and 10% during the 2031–2060 and 2066–2095 periods, respectively. Based on the future population data from the SSP2 scenario, the average annual exposed population to landslides increases by 90% and 80% during the 2031–2060 and 2066–2095 periods, respectively, compared to the 1971–2000 period.

(2) Due to the impacts of extreme precipitation under the climate change scenario, the global casualty risk of landslides is expected to present a growing trend. The average annual casualties caused by global landslides were projected to increase from 3240 during the 1971–2000 period to 7670 and 8380 during the 2031–2060 and 2066–2095 periods, with growth rates of 140% and 160% respectively, under the SSP2-4.5 scenario.

(3) The top 10 countries with high casualty risks to landslide disasters are China, Afghanistan, India, the Philippines, Indonesia, Rwanda, Turkey, Nepal, Guatemala, and Brazil, and the average annual casualties for each of these countries are over 220 during the 2066–2095 period under the SSP2-4.5 scenario. The high susceptibility to landslides has a significant impact on casualties in Nepal and Guatemala. Countries such as China, Afghanistan, and India are primarily affected by high population exposure to future landslide disasters. The high casualty risk in Turkey is mainly influenced by high vulnerability to landslide disasters. The high casualty risk in Rwanda, the Philippines and Brazil is affected by both a highly exposed population and a high vulnerability to landslides.

**Acknowledgments** The Second Tibetan Plateau Scientific Expedition and Research Program (STEP, Grant No. 2019QZKK0906) and National Key Research and Development Program of China (Grant No. 2023YFC3007204) supported this work. We are grateful for the support of this program.



## References

Alvioli, M., M. Melillo, F. Guzzetti, M. Rossi, E. Palazzi, J. Von Hardenberg, M.T. Brunetti, and S. Peruccacci. 2018. Implications of climate change on landslide hazard in Central Italy. *Science of the Total Environment* 630: 1528–1543.

Barros, V.R., C.B. Field, D.J. Dokken, M.D. Mastrandrea, K.J. Mach, T.E. Bilir, M. Chatterjee, K.L. Ebi, et al. 2014. Climate change 2014: Impacts, adaptation, and vulnerability. Part B: Regional aspects. *Contribution of Working Group II to the Fifth Assessment Report of the Intergovernmental Panel on Climate Change*. Cambridge, UK: Cambridge University Press.

Budimir, M.E.A., P.M. Atkinson, and H.G. Lewis. 2015. A systematic review of landslide probability mapping using logistic regression. *Landslides* 12(3): 419–436.

Buma, J., and M. Dehn. 2000. Impact of climate change on a landslide in South East France, simulated using different GCM scenarios and downscaling methods for local precipitation. *Climate Research* 15(1): 69–81.

Caine, N. 1980. The rainfall intensity: Duration control of shallow landslides and debris flows. *Geografiska Annaler: Series A, Physical Geography* 62(1–2): 23–27.

Ciabatta, L., S. Camici, L. Brocca, F. Ponziani, M. Stelluti, N. Berni, and T. Moramarco. 2016. Assessing the impact of climate-change scenarios on landslide occurrence in Umbria Region, Italy. *Journal of Hydrology* 541: 285–295.

Coe, J.A. 2012. Regional moisture balance control of landslide motion: Implications for landslide forecasting in a changing climate. *Geomorphology* 40(4): 323–326.

Collison, A., S. Wade, J. Griffiths, and M. Dehn. 2000. Modelling the impact of predicted climate change on landslide frequency and magnitude in SE England. *Engineering Geology* 55(3): 205–218.

CRED (Centre for Research on the Epidemiology of Disasters). 2019. Emergency Events Database (EM-DAT). https://www.emdat.be/. Accessed 10 Sept 2020.

Crozier, M.J. 2010. Deciphering the effect of climate change on landslide activity: A review. *Geomorphology* 124(3–4): 260–267.

Dixon, N., and E. Brook. 2007. Impact of predicted climate change on landslide reactivation: Case study of Mam Tor. *UK. Landslides* 4(2): 137–147.

Emberson, R., D. Kirschbaum, and T. Stanley. 2020. New global characterization of landslide exposure. *Natural Hazards and Earth System Sciences* 20(12): 3413–3424.

Farahmand, A., and A. AghaKouchak. 2013. A satellite-based global landslide model. *Natural Hazards and Earth System Sciences* 13(5): 1259–1267.

Froude, M.J., and D.N. Petley. 2018. Global fatal landslide occurrence from 2004 to 2016. *Natural Hazards and Earth System Sciences* 18(8): 2161–2181.

Gariano, S.L., and F. Guzzetti. 2016. Landslides in a changing climate. *Earth-Science Reviews* 162: 227–252.

Gariano, S.L., and F. Guzzetti. 2022. Mass-movements and climate change. In *Treatise on geomorphology*, 2nd edn, ed. J.F. Shroder, 546–558. San Diego, CA: Academic Press.

Gariano, S.L., G. Rianna, O. Petrucci, and F. Guzzetti. 2017. Assessing future changes in the occurrence of rainfall-induced landslides at a regional scale. *Science of the Total Environment* 596–597: 417–426.

Globcover 2000 (Global Land Cover 2000 database). European Commission, Joint Research Centre. https://joint-research-centre.ec.europa.eu/scientific-tools-databases_en. Accessed 27 Dec 2020.

Gómez, D., E.F. García, and E. Aristizábal. 2023. Spatial and temporal landslide distributions using global and open landslide databases. *Natural Hazards* 117(1): 25–55.

Guzzetti, F., S.L. Gariano, S. Peruccacci, M.T. Brunetti, I. Marchesini, M. Rossi, and M. Melillo. 2020. Geographical landslide early warning systems. *Earth-Science Reviews* 200: Article 102973.

Hong, Y., R. Adler, and G. Huffman. 2007. Use of satellite remote sensing data in the mapping of global landslide susceptibility. *Natural Hazards* 43(2): 245–256.

Hungr, O., S. Leroueil, and L. Picarelli. 2014. The Varnes classification of landslide types, an update. *Landslides* 11(2): 167–194.

Hürlimann, M., Z. Guo, C. Puig-Polo, and V. Medina. 2022. Impacts of future climate and land cover changes on landslide susceptibility: Regional scale modelling in the Val d'Aran region (Pyrenees, Spain). *Landslides* 19(1): 99–118.

IPCC (Intergovernmental Panel on Climate Change). 2011. *Managing the risks of extreme events and disasters to advance climate change adaptation (SREX)*. Cambridge, UK: Cambridge University Press.

IPCC (Intergovernmental Panel on Climate Change). 2021. Summary for policymakers. In *Climate change 2021: The physical science basis. Contribution of Working Group I to the Sixth assessment report of the Intergovernmental Panel on Climate Change*. Cambridge, UK: Cambridge University Press.

Jaedicke, C., M. Van Den Eeckhaut, F. Nadim, J. Hervás, B. Kalsnes, B.V. Vangelsten, J.T. Smith, and V. Tofani et al. 2014. Identification of landslide hazard and risk "hotspots" in Europe. *Bulletin of Engineering Geology and the Environment* 73: 325–339.

Jakob, M., and S. Lambert. 2009. Climate change effects on landslides along the southwest coast of British Columbia. *Geomorphology* 107(3–4): 275–284.

Jia, G.Q., M. Alvioli, S.L. Gariano, I. Marchesini, F. Guzzetti, and Q.H. Tang. 2021. A global landslide non-susceptibility map. *Geomorphology* 389: Article 107804.

Kharin, V.V., F.W. Zwiers, X. Zhang, and M. Wehner. 2013. Changes in temperature and precipitation extremes in the CMIP5 ensemble. *Climatic Change* 119(2): 345–357.

Kirschbaum, D.B., and T. Stanley. 2018. Satellite-based assessment of rainfall-triggered landslide hazard for situational awareness. *Earth's Future* 6(3): 505–523.

Kirschbaum, D.B., R. Adler, Y. Hong, S. Hill, and A. Lerner-Lam. 2010. A global landslide catalog for hazard applications: Method, results, and limitations. *Natural Hazards* 52(3): 561–575.

Kirschbaum, D.B., T. Stanley, and Y. Zhou. 2015. Spatial and temporal analysis of a global landslide catalog. *Geomorphology* 249: 4–15.

Lin, L., Q.G. Lin, and Y. Wang. 2017. Landslide susceptibility mapping on a global scale using the method of logistic regression. *Natural hazards and Earth System Sciences* 17(8): 1411–1424.

Lin, Q.G., and Y. Wang. 2018. Spatial and temporal analysis of a fatal landslide inventory in China from 1950 to 2016. *Landslides* 15(12): 2357–2372.

Lin, Q.G., S. Steger, M. Pittore, J. Zhang, L. Wang, T. Jiang, and Y. Wang. 2022. Evaluation of potential changes in landslide susceptibility and landslide occurrence frequency in China under climate change. *Science of the Total Environment* 850: Article 158049.

Lin, Q.G., Y. Wang, T. Glade, J.H. Zhang, and Y. Zhang. 2020. Assessing the spatiotemporal impact of climate change on event rainfall characteristics influencing landslide occurrences based on multiple GCM projections in China. *Climatic Change* 162(2): 761–779.

Liu, Y.J., J. Chen, T. Pan, Y.H. Liu, Y. Zhang, Q.S. Ge, P. Ciais, and J. Penuelas. 2020. Global socioeconomic risk of precipitation extremes under climate change. *Earth's Future* 8(9): Article e2019EF001331.

Ma, S.Y., X.Y. Shao, and C. Xu. 2023. Physically-based rainfall-induced landslide thresholds for the Tianshui area of Loess Plateau, China by TRIGRS model. *Catena* 233: Article 1107499.

Mandapaka, P.V., and E.Y.M. Lo. 2018. Assessment of future changes in Southeast Asian precipitation using the NASA Earth Exchange Global Daily Downscaled Projections data set. *International Journal of Climatology* 38(14): 5231–5244.

Melchiorre, C., and P. Frattini. 2012. Modelling probability of rainfall-induced shallow landslides in a changing climate, Otta. *Central Norway. Climatic Change* 113(2): 413–436.

Nadim, F., C. Jaedicke, H. Smebye, and B. Kalsnes. 2013. Assessment of global landslide hazard hotspots. In *Landslides: Global risk preparedness*, ed. K. Sassa, B. Rouhban, S. Briceño, M. McSaveney, and B. He, 59–71. Berlin: Springer.

Nadim, F., O. Kjekstad, P. Peduzzi, C. Herold, and C. Jaedicke. 2006. Global landslide and avalanche hotspots. *Landslides* 3(2): 159–173.

O'Neill, B.C., E. Kriegler, K.L. Ebi, E. Kemp-Benedict, K. Riahi, D.S. Rothman, B.J. van Ruijven, D.P. van Vuuren, and J. Birkmann. 2017. The roads ahead: Narratives for shared socioeconomic pathways describing world futures in the 21st century. *Global Environmental Change* 42: 169–180.

O'Neill, B.C., E. Kriegler, K. Riahi, K.L. Ebi, S. Hallegatte, T.R. Carter, R. Mathur, and D.P. van Vuuren. 2014. A new scenario framework for climate change research: The concept of shared socioeconomic pathways. *Climatic Change* 122(3): 387–400.

Parry, M.L., O.F. Canziani, J.P. Palutikof, P.J. Van der Linden, and C.E. Hanson. 2007. Climate change 2007: Impacts, adaptation and vulnerability. *Contribution of Working Group II to the Fourth Assessment Report of the Intergovernmental Panel on Climate Change*. Cambridge, UK: Cambridge University Press.

Pecoraro, G., M. Calvello, and L. Piciullo. 2019. Monitoring strategies for local landslide early warning systems. *Landslides* 16(2): 213–231.

Petley, D.N. 2012. Global patterns of loss of life from landslides. *Geology* 40(10): 927–930.

Petley, D.N., G.J. Hearn, A. Hart, N.J. Rosser, S.A. Dunning, K. Oven, and W.A. Mitchell. 2007. Trends in landslide occurrence in Nepal. *Natural Hazards* 43(1): 23–44.

Piciullo, L., M. Calvello, and J.M. Cepeda. 2018. Territorial early warning systems for rainfall-induced landslides. *Earth-Science Reviews* 179: 228–247.

Rianna, G., A. Zollo, P. Tommasi, M. Paciucci, L. Comegna, and P. Mercogliano. 2014. Evaluation of the effects of climate changes on landslide activity of Orvieto clayey slope. *Procedia Earth and Planetary Science* 9: 54–63.

Rong, G.Z., K.W. Li, Z.J. Tong, X.P. Liu, J.Q. Zhang, Y.C. Zhang, and T.T. Li. 2023. Population amount risk assessment of extreme precipitation-induced landslides based on integrated machine learning model and scenario simulation. *Geoscience Frontiers* 14(3): Article 101541.

Sooraj, K.P., P. Terray, and P. Xavier. 2015. Sub-seasonal behaviour of Asian summer monsoon under a changing climate: Assessments using CMIP5 models. *Climate Dynamics* 46(11): 4003–4025.

Stanley, T., and D.B. Kirschbaum. 2017. A heuristic approach to global landslide susceptibility mapping. *Natural Hazards* 87(1): 145–164.

Turkington, T., A. Remaître, J. Ettema, H. Hussin, and C. Van Westen. 2016. Assessing debris flow activity in a changing climate. *Climatic Change* 137(1–2): 293–305.

Van Den Eeckhaut, M., and J. Hervás. 2012. State of the art of national landslide databases in Europe and their potential for assessing landslide susceptibility, hazard and risk. *Geomorphology* 139: 545–558.

Villani, V., G. Rianna, P. Mercogliano, and A.L. Zollo. 2015. Statistical approaches versus weather generator to downscale RCM outputs to slope scale for stability assessment: A comparison of performances. *Journal of Geotechnical and Geoenvironmental Engineering* 20: 1495–1515.

Westra, S., H.J. Fowler, J.P. Evans, L.V. Alexander, P. Berg, F. Johnson, E.J. Kendon, G. Lenderink, and N.M. Roberts. 2014. Future changes to the intensity and frequency of short-duration extreme precipitation. *Reviews of Geophysics* 52: 522–555.

Yang, W.T., L.L. Shen, and P.J. Shi. 2015. Mapping landslide risk of the world. In *World atlas of natural disasters risk*, 57–66. Berlin: Springer.

Zhang, Y., Y. Wang, Y. Chen, Y.J. Xu, G.M. Zhang, Q.G. Lin, and R.H. Luo. 2021. Projection of changes in flash flood occurrence under climate change at tourist attractions. *Journal of Hydrology* 595: Article 126039.